PHYSICAL REVIEW B **93**, 144109 (2016)

Strain coupling, microstructure dynamics, and acoustic mode softening in germanium telluride

D. Yang,[1,2] T. Chatterji,[3] J. A. Schiemer,[1] and M. A. Carpenter[1]

[1]*Department of Earth Sciences, University of Cambridge, Cambridge CB2 3EQ, United Kingdom*

[2]*School of Materials Science and Technology, China University of Geosciences, Beijing 100083, People's Republic of China*

[3]*Institut Laue-Langevin, 71 Avenue des Martyrs, CS 20156, 38042 Grenoble Cedex 9, France*

(Received 23 December 2015; revised manuscript received 26 February 2016; published 11 April 2016)

GeTe is a material of intense topical interest due to its potential in the context of phase-change and nanowire memory devices, as a base for thermoelectric materials, and as a ferroelectric. The combination of a soft optic mode and a Peierls distortion contributes large strains at the cubic-rhombohedral phase transition near 625 K and the role of these has been investigated through their influence on elastic and anelastic properties by resonant ultrasound spectroscopy. The underlying physics is revealed by softening of the elastic constants by ∼30%–45%, due to strong coupling of shear and volume strains with the driving order parameter and consistent with an improper ferroelastic transition which is weakly first order. The magnitude of the softening is permissive of the transition mechanism involving a significant order/disorder component. A Debye loss peak in the vicinity of 180 K is attributed to freezing of the motion of ferroelastic twin walls and the activation energy of ∼0.07 eV is attributed to control by switching of the configuration of long and short Ge-Te bonds in the first coordination sphere around Ge. Precursor softening as the transition is approached from above can be described with a Vogel-Fulcher expression with a similar activation energy, which is attributed to coupling of acoustic modes with an unseen central mode that arises from dynamical clusters with local ordering of the Peierls distortion. The strain relaxation and ferroelastic behavior of GeTe depend on both displacive and order/disorder effects but the dynamics of switching will be determined by changes in the configuration of distorted $GeTe_6$ octahedra, with a rather small activation energy barrier.

DOI: 10.1103/PhysRevB.93.144109

I. INTRODUCTION

GeTe is a remarkable material in several topical contexts, including as an end-member phase for crystal-to-amorphous phase change memory [1–4], for nanowire memory devices [5], as a base for thermoelectric materials [6,7], and as a ferroelectric at room temperature which retains "a reversible, size dependent polar-nonpolar transition in nanocrystal ensembles" [8]. Close interest arises because of the particular combination of structure and electronic properties which can give fast switching and stable storage. These in turn depend on high vacancy substitution for Ge [9,10] and a Peierls-type distortion of the Ge-Te coordination which persists even above the melting point [3,11–14]. The Peierls distortion can also be described as a second order Jahn-Teller distortion of the first coordination sphere of Te around Ge, due to the formation of Te lone pairs [15].

In addition to the implications for device applications, there has been controversy in relation to the origin of ferroelectric properties that arise at a cubic ($Fm\bar{3}m$)-rhombohedral ($R3m$) phase transition at ∼600–700 K [7,14,16–19] because the electronic instability which gives rise to the Peierls distortion would give the same change in symmetry as a soft optic mode. A classical displacive transition driven by a zone center optic mode was implied by Raman scattering results, which showed mode softening up to at least 500 K [18] and would be consistent with the equivalent transition observed at lower temperatures in $Sn_xGe_{1-x}Te$ [20] and $Pb_xGe_{1-x}Te$ [21]. This displacive mechanism was supported by theory [19], by inelastic neutron scattering data from a powder sample, and by computer simulations [22]. However, probes of the local structure have shown that the Peierls distortion persists locally in the structure at all temperatures up to the melting point and, hence, that the transition must involve at least some order/disorder of distorted units [13–15].

Conventional memory devices depend on switching, with characteristic mechanisms that involve movement of twin walls in response to an applied field. In the case of GeTe, the mechanism of ferroelectric switching will depend at a local scale on reversing the topology of the three long and three short bonds of individual distorted $GeTe_6$ octahedra [23]. As well as being ferroelectric, the phase transition in GeTe is improper ferroelastic, however, and it is inevitable that the rhombohedral phase will contain ferroelastic (71/109°) twin walls which will also move under an applied electric field, though with different dynamics from 180° twin walls. This is normal in ferroelectrics such as $BaTiO_3$ and $Pb(Zr,Ti)O_3$ but leads to the expectation that GeTe must also display diverse acoustic properties which have not yet been investigated. The primary objective of the present study was to use measurements of elastic and anelastic properties to reveal the phenomenological richness and underlying physics of a material which, superficially at least, is just a binary compound with the rocksalt structure.

Here we show, first, that softening of the shear elastic constants due to classical strain/order parameter coupling is consistent with a predominantly displacive mechanism for the proper ferroelectric/improper ferroelastic transition, but with significant contribution from order/disorder. Second, we argue that precursor softening in the stability field of the cubic structure provides indirect evidence of a central relaxational mode which arises from some dynamical microstructure of polar nanoregions or tweed and which couples with acoustic modes. Finally, we suggest that the activation energy of

~0.1 eV extracted from both a peak in the acoustic loss due to freezing of ferroelastic twin walls near 200 K, which is consistent with formalism from the Debye equations [24], and from a Vogel-Fulcher description of the precursor softening, is due to motion of Ge between the two alternative sites of the Peierls structure. This is likely to be fundamental to the dynamical response of GeTe to external fields.

II. STRAIN ANALYSIS

From the perspectives of strain and elasticity, the weakly first order cubic-rhombohedral transition in GeTe appears to have all the typical features of being improper ferroelastic. A formal strain analysis, based on a Landau expansion with strain/order parameter coupling using lattice parameter data from the literature, is given in the Appendix. Values of the symmetry breaking shear strain e_4 and volume strain e_a are ~3% and ~1.8% at room temperature, signifying strain coupling comparable in strength to that which accompanies Jahn-Teller transitions in perovskites such as $LaMnO_3$ [25], but stronger by a factor of ~10 than accompanies octahedral tilting transitions in perovskites such as $SrZrO_3$ [26]. Variations of these strains with temperature can be represented by the standard solution to a Landau 2-4-6 potential for a weakly first order displacive transition, i.e., with negative fourth order coefficient and a small difference between the transition temperature T_{tr} and critical temperature T_c.

III. EXPERIMENTAL DETAILS

The elastic and anelastic properties of a single crystal sample cut in the shape of a rectangular parallelepiped ($1.977 \times 3.283 \times 4.611\,mm^3$, 0.1822 g, but with no particular crystallographic orientation) were measured by resonant ultrasound spectroscopy (RUS). Different pieces of the same boule had previously been used for neutron diffraction [17] and synchrotron x-ray diffraction [15]. Examination of one or the off-cuts by electron backscatter diffraction (EBSD) confirmed that it was a single crystal.

The RUS method has been described in detail elsewhere [27]. Low-temperature data were collected using dynamic resonance system (DRS) "modulus II" electronics and an orange helium-flow cryostat, as described by McKnight *et al.* [28]. The sample was held across a pair of faces directly between the transducers. The automated sequence involved collection of spectra at 30 K intervals during cooling from ~305 to ~5 K, with a period of 20 min allowed for thermal equilibration at each temperature. This was followed by heating between ~5 and ~300 K, with data collection at 5 K intervals and the same thermal equilibration period at each temperature. Each spectrum contained 65 000 data points in the frequency range 100–1200 kHz. Measured temperatures are believed to be accurate to within ±1 K, and temperature stability during data collection is better than ±0.1 K.

High-temperature spectra were collected with the sample balanced across a pair of corners between the tips of two alumina rods protruding into a horizontal tube furnace. In this system the transducers are on the ends of the rods, outside the furnace, as described by McKnight *et al.* [29], and spectra are collected using Stanford electronics [30]. Temperature is monitored by a thermocouple sited within a few millimeters of the sample and checked from time to time against the α-β transition temperature of quartz, giving an experimental uncertainty of ±~1 K. Spectra were collected in heating and cooling sequences, from ~300 to ~560 K with ~20 K steps, from ~560 to ~650 K with 2 K steps, from ~650 to ~750 K with 5 K steps, and then from ~750 to ~650 K with 5 K steps, from ~650 to ~560 K with 2 K steps, from ~560 to ~300 K with ~10 K steps. A period of 20 min was again allowed for thermal equilibration at each temperature. Individual spectra contained 65 000 data points in the frequency range 50–1200 kHz.

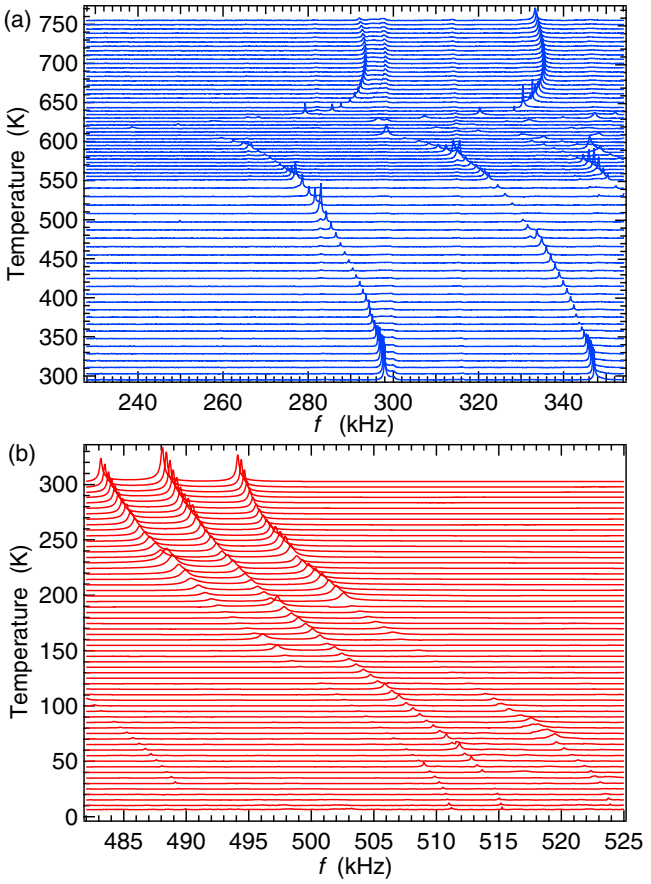

FIG. 1. Segments of RUS spectra collected from a rectangular parallelepiped of GeTe with dimensions $1.977 \times 3.283 \times 4.611\,mm^3$ and mass 0.1822 g. Each spectrum has been offset up the y axis in proportion to the temperature at which it was collected. (a) Cooling sequence, ~760 K to room temperature. (b) Heating sequence, ~7 K to room temperature.

IV. RESULTS

Segments of the primary RUS spectra collected during cooling through the phase transition (Fig. 1) show sharp resonance peaks all stiffening (increasing in frequency f)

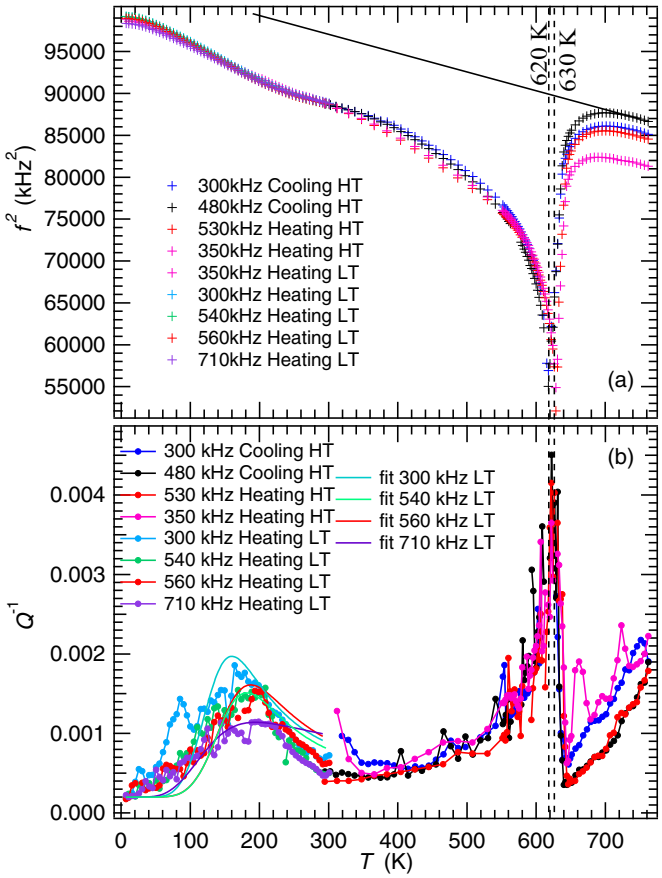

FIG. 2. (a) Temperature dependence of f^2 for selected resonances, scaled to overlap near room temperature. A small hysteresis of the transition point between heating (∼630 K) and cooling (∼620 K) indicates weak first order character. The straight line is a fit to data collected at the highest temperatures and extrapolated to lower temperatures in order to represent reference values f_o^2 of the cubic structure. (b) Temperature dependence of Q^{-1} from selected resonances, showing a marked break in trend at ∼650 K, a peak in the vicinity of the minimum in f^2, and frequency-dependent maxima near 180 K.

slightly with decreasing temperature from ∼760 K down to ∼700 K, and then softening steeply to a minimum at ∼620 K, which is taken to be the transition point. The softening trend then reverses and stiffening occurs down to the lowest temperature reached (7 K). The width at half maximum height Δf of all the peaks broaden immediately below the transition point [Fig. 1(a)] and there is an additional interval of peak broadening below ∼200 K [Fig. 1(b)].

Fitting of selected peaks provides a quantitative picture of the qualitative patterns shown by the primary spectra (Fig. 2). Variations of f^2 give the temperature dependence of predominantly shear elastic constants, and $Q^{-1}(=\Delta f/f)$ is a measure of acoustic loss. The total amount of softening with respect to the parent cubic structure is ∼45% at the transition point but reduces to a more nearly constant value of ∼30% at lower temperatures [Fig. 2(a)]. This form of nonlinear recovery below T_{tr} (∼620 K on cooling and ∼630 K on heating), is closely similar to that expected for tricritical evolution of the order parameter (e.g., Refs. [26,31]).

V. DISCUSSION

A. Order/disorder component

From Landau theory, the excess entropy for a phase transition is given by $-a/2$, where a is the coefficient for the second order term in the order parameter q. The change in heat capacity at $T = T_c$, $\Delta C_{p,Tc}$, of the second order transition in SnTe is $\sim 0.5\,\mathrm{J\,mol^{-1}\,K^{-1}}$ [32]. For an excess free energy given by $\frac{1}{2}a(T - T_c)q^2 + \frac{1}{4}bq^4$, the excess heat capacity varies as $aT/2T_c$ [33], so that $a = 2\Delta C_{p,Tc} =\sim 1\,\mathrm{J\,mol^{-1}\,K^{-1}}$. The total excess entropy for the change from $q = 0$ to $q = 1$ is then $\sim -0.5\,\mathrm{J\,mol^{-1}\,K^{-1}}$, which would be typical of a displacive transition mechanism. At small values of x in $Sn_xGe_{1-x}Te$, the transition remains second order [20,32,34] and a classic steplike softening of elastic constants is observed, fitting with expectations for the displacive limit to which Landau theory refers [35–37]. ΔC_p increases with increasing Ge content [34], however, implying that the excess entropy also increases, as would be expected if there is an increasing configurational contribution. Estimates of the magnitude of the excess entropy from integration of the excess heat capacity for GeTe samples with a range of stoichiometries are in the range $0.9 - 3.1\,\mathrm{J\,mol^{-1}\,K^{-1}}$ [38], though this is still less than the expected value of $-R\ln 2 = -5.8\,\mathrm{J\,mol^{-1}\,K^{-1}}$ for the simplest AB ordering process.

Following Slonczewski and Thomas [39], the magnitude of softening at a second order transition with strain e coupled as λeq^2 scales approximately with λ^2/b, where the value of the b coefficient is approximately aT_c. Antiferromagnetic ordering in CoF_2 below ∼39 K has an excess entropy close to $-R\ln 2$ and is accompanied by spontaneous strains of ∼0.001% and ∼3% softening of the shear modulus [40]. To first approximation, allowing for the same configurational entropy, an order of magnitude increase in λ and an order of magnitude increase in T_c should lead to an order of magnitude increase in the amount of softening in GeTe, which is essentially what is observed. In other words, the elastic softening is permissive of a high excess entropy, consistent with a significant configurational component. Moreover, the simplest model for order/disorder gives an evolution of the order parameter which is not so far from tricritical in form [40].

B. Acoustic loss

Q^{-1} values at first reduce with falling temperature but have a sharp increase below ∼644 K on heating and ∼640 K on cooling towards maxima which, within experimental uncertainty, coincide with the minima in f^2 [Fig. 2(b)]. Variations of Q^{-1} below T_{tr} also display typical aspects of the patterns of anelastic loss seen at improper ferroelastic transitions in perovskites. The peak at T_{tr} closely resembles the peak seen at the transition temperature for octahedral tilting in $EuTiO_3$ [41,42], $SrZrO_3$ [26], and $Ca_{0.2}Sr_{0.8}TiO_3$ [43]. The plateau of high Q^{-1} between ∼500 and ∼300 K results from the motion under external stress of ferroelastic twin walls in an effectively viscous medium. Finally, the frequency-dependent Debye peak at ∼180 K is typical of the effects of pinning of the twin walls by defects through some freezing interval, as seen for the tilting transition in $KMnF_3$ [44] and for the ferroelectric transition in $Pb(In_{1/2}Nb_{1/2})O_3 - Pb(Mg_{1/3}Nb_{2/3})O_3$-$PbTiO_3$ [45].

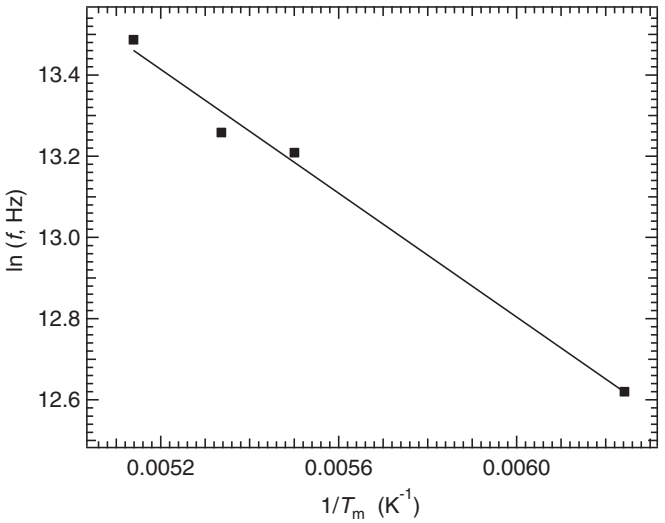

FIG. 3. Arrhenius plot of frequency f versus $1/T_m$, from the data of Table I. An activation energy $U = 0.066 \pm 0.005$ eV is obtained from the slope and $\tau_o = 2.8 \times 10^{-8} \pm \sim 1 \times 10^{-8}$ s from one over the intercept.

Similar patterns of acoustic loss are seen at lower frequencies in $LaAlO_3$ and $(Ca,Sr)TiO_3$, where the overall behavior is due to forward and back motion of the needle tips of ferroelastic twin walls, and the freezing mechanism is essentially pinning of the twin walls by oxygen vacancies [46–49]. Under the low stress and higher frequency conditions of an RUS experiment, the twin wall displacement mechanism most likely involves lateral motions of ledges along the length of the walls [50–52]. For present purposes, values of the temperatures T_m at which the Debye loss peaks in Fig. 2(b) have a maximum Q_m^{-1}, were first determined by fitting a polynomial function to data between ∼10 and ∼300 K. A thermally activated loss mechanism with relaxation time τ given by the condition $\omega\tau = 1$ (angular frequency $\omega = 2\pi f$) at T_m is expected to follow $\tau = \tau_o \exp(U/k_B T)$; U is the activation energy, τ_o is the reciprocal of the attempt frequency, and k_B is the Boltzmann constant. An Arrhenius plot gives $U/k_B = 763 \pm 53$ K ($U = 0.066 \pm 0.005$ eV) and $\tau_o = 3 \pm 1 \times 10^{-8}$ s (Fig. 3). This value of U is close to the activation energy barrier of 0.11 eV obtained by DFT calculation for a switching process that involves swapping of shorter and longer Ge-Te bonds in which the Ge atoms move by ∼0.3 Å [23]. The experimental result therefore appears to confirm the suggestion in Ref. [23] that such movements could be important in the mechanism of domain wall movement. Mechanisms involving vacancies can probably be ruled out on the basis that activation energies for diffusion of Ge in GeTe are expected to have values $\geqslant \sim 1$ eV [53].

Each Debye loss peak can also be fit using the expression [44,52,54,55]

$$Q^{-1}(T) = Q_m^{-1}\left[\cosh\left\{\frac{U}{k_B r_2(\beta)}\left(\frac{1}{T} - \frac{1}{T_m}\right)\right\}\right]^{-1}, \quad (1)$$

where $r_2(\beta)$ relates to the width of a Gaussian spread of relaxation times. The parameter β is a measure of the width of the Gaussian distribution, as illustrated in Fig. 4 of Nowick and Berry [24], and is zero for a standard anelastic solid. Fits of this expression to the data have been added to Fig. 2(a) and give values of $U/k_B r_2(\beta)$ in the range ∼350–650 K. If $U = 0.066$ eV is assumed from the simpler treatment, the fits give $r_2(\beta)$ in the range 1.2–2.2, with the value near ∼2 being poorly constrained (Table I). The implication is that there is a single pinning mechanism with only a small spread of relaxation times [$\beta \sim 0$, $r_2(\beta) \sim 1$].

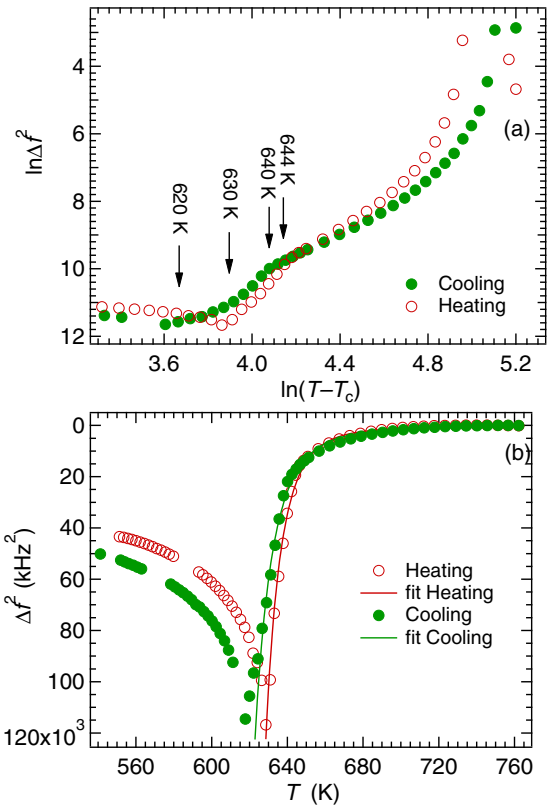

FIG. 4. Variations of $\Delta f^2 = (f_o^2 - f^2)$ with temperature. (a) The data above the transition temperature do not have a linear temperature dependence with slope between $-1/2$ and -2, as would be expected for a power-law description for $T_c = 581$ K. (b) Curves through the data above T_{tr} are fits of a Vogel-Fulcher equation.

C. Precursor softening dynamics

Precursor softening of the elastic constants as an improper ferroelastic transition point is approached from above provides insights into dynamic effects because linear/quadratic coupling between the nonzero strains and the driving order parameter does not contribute any softening when $q = 0$. Fluctuations

TABLE I. Fit parameters for Debye-like loss peaks.

Frequency at T_m(Hz)	T_m(K)	Q_m^{-1}	$r_2(\beta)$	U (eV)
302 640	160.2	0.001 77	1.4 ± 0.1	0.066
545 230	181.8	0.001 31	1.2 ± 0.1	0.066
572 820	187.4	0.001 41	1.2 ± 0.2	0.066
719 710	194.6	0.000 94	2.2 ± 0.3	0.066

relating to dispersion of the soft mode can be responsible and would be expected to conform to a phenomenological description of the form $\Delta C_{ik} = A_{ik}(T - T_c)^{-\kappa}$, where ΔC_{ik} is the amount of softening of single crystal elastic constants and A_{ik} is a material constant. The value of the exponent κ, between 1/2 and 2, depends on the anisotropy and dispersion of soft branches round the critical point of the soft mode [31,56–59].

Alternatively, the dynamical effects ahead of a ferroelectric transition can be due to the development of polar nanoregions. These are purely dynamic immediately below the Burns temperature but can become quasistatic at a temperature T^* before they freeze. Softening of the shear modulus occurring in this way in $Pb(Mg_{1/3}Nb_{2/3})O_3$ [60] and $Pb(Sc_{0.5}Ta_{0.5})O_3$ [61] can be represented by a Vogel-Fulcher expression $\Delta C_{ik} = A_{ik}\exp[U/k_B(T - T_{VF})]$, where T_{VF} is the zero-frequency freezing temperature. The extent of precursor softening for GeTe is expressed here as $\Delta f^2 = (f_o^2 - f^2)$, where f_o^2 is the square of the resonance frequency obtained from a linear fit to the highest temperature data, extrapolated down to T_{tr} [Fig. 2(a)]. Δf^2 for resonances with frequency near 530 kHz (heating sequence) or 480 kHz (cooling sequence) at room temperature are shown in Fig. 4. The power-law description, with a value of $T_c = 581$ K taken from the strain analysis of data from Ref. [15], would not provide a good description [Fig. 4(a)] but the Vogel-Fulcher expression with $U = 0.10 \pm 0.06$ eV and $T_{VF} = 520 \pm 30$ or $T_{VF} = 530 \pm 30$ K can for heating or cooling, respectively [Fig. 4(b)]. Remarkably, the activation energy for the fits is almost the same as for domain wall freezing, which appears to imply that the energy barrier associated with the freezing process is also determined by changing the configuration of short and long Ge-Te bonds.

We propose that the precursor elastic softening seen in all mechanical resonances of the GeTe sample reflects coupling of the acoustic modes with a central relaxational mode due to dynamical clustering of polar regions in the manner reported recently for the ferroelectric transition in $Pb(Fe_{0.5}Nb_{0.5})O_3$ [62]. The central mode would involve flipping of the polarization or displacements of boundaries between ordered clusters, and T_{VF} represents the temperature at which this motion would be expected to cease if the ferroelectric transition did not intervene. A test would be observation of a mode (or modes) with relaxation times perhaps in the vicinity of $\sim 10^{-10}$ s, as appears to have been detected in terahertz spectra by Kadlec *et al.* [63]. Such a central mode would also be expected to couple with optic modes which might therefore provide indirect evidence of its unseen presence. There is a distinct kink in the Δf^2 data at ~640–645 K during both heating and cooling [Fig. 4(a)], and this is interpreted as representing the temperature T^* where the clusters acquire some static component. The change in trend of Δf^2 coincides with the abrupt change in trend for Q^{-1} [Fig. 2(b)], as would be expected if it marks the development of some ferroelastic microstructure with falling temperature—for which the most likely form would be tweed. Some degree of strain coupling of the dynamical clustering at $T > T^*$ is evidenced by the persistence of relatively high values of Q^{-1} up to the highest temperatures of the measurements presented here.

The acoustic data complement the evidence of clustering from pair distribution analysis of diffraction data presented in Ref. [15]. The sample used in the present study is from the same original boule and close agreement for the transition temperature implies that the compositions are closely similar. Hudspeth *et al.* [15] described ordered clusters with dimension ~20 Å in the stability field of the cubic structure, with a steep increase in correlation length between 650 and 500 K. This interval coincides almost exactly with the interval over which Q^{-1} shows a peak through the transition. Correlations of the distorted GeTe polyhedra can therefore be understood as being at first dynamic on the cluster length scale and then quasistatic below ~645 K when the length scale of the correlations starts to increase. As pointed out already by Chatterji *et al.* [16], the positive volume strain observed for GeTe has essentially the same form as seen in $LaMnO_3$ where the transition mechanism involves ordering of MnO_6 octahedra with Jahn-Teller distortions.

VI. CONCLUSIONS

Elastic and anelastic anomalies provide a sensitive window on the strength and dynamics of strain coupling effects which accompany structural, magnetic, and electronic phase transitions in perovskites [52]. In the case of GeTe, large softening of the shear elastic constants and strong coupling of the driving order parameter(s) with shear strain are consistent with improper ferroelastic character for the $Fm\bar{3}m$-$R3m$ transition. The temperature dependence of the strain evolution and the form of the elastic softening is consistent with a mean field description of a displacive transition which is close to tricritical. The magnitude of the softening, however, is permissive of a significant configurational component coming from order/disorder of distorted GeTe polyhedra. The softening data also provide evidence for the influence of an unseen central relaxational mode. An activation energy barrier of ~0.1 eV seems to control both the dynamics of the ordering process and of the resulting ferroelastic microstructures. As such it is likely to represent the thermal barrier for switching processes.

GeTe already has remarkable macroscopic properties but the existence of polar domains, tweed microstructures, and possible combinations of 180° and 71/109° twin walls opens up additional possibilities in the context of domain engineering and the use of transformation microstructures for providing device properties [64,65]. For example, the proximity to a metal-insulator transition [5], due to the particular coupling between atomic structure and electronic structure, means that is inevitable that the electrical properties of twin walls will differ from those of the domains.

ACKNOWLEDGMENTS

RUS facilities have been established and maintained in Cambridge through grants from the Natural Environment Research Council and the Engineering and Physical Sciences Research Council of Great Britain to MAC (NE/B505738/1, NE/F17081/1, EP/I036079/1). Dexin Yang thanks the China Scholarship Council.

APPENDIX: SYMMETRY AND STRAIN ANALYSIS

Ferroelectric dipoles typically develop in GeTe due to displacements of Ge and Te atoms following the evolution

of order parameter components that belong to the irreducible representation Γ_4^- of parent space group $Fm\bar{3}m$. As well as being ferroelectric at room temperature, GeTe is in principle improper ferroelastic due to coupling of the Γ_4^- order parameter with strain. Following Rehwald and Lang [35] and Sugai *et al.* [21], the Landau expansion for the excess free energy G, including saturation, is

$$\begin{aligned} G = {} & \frac{1}{2}a\Theta_s\left[\coth\left(\frac{\Theta_s}{T}\right) - \coth\left(\frac{\Theta_s}{T_c}\right)\right]\left(q_1^2+q_2^2+q_3^2\right) \\ & +\frac{1}{4}b\left(q_1^2+q_2^2+q_3^2\right)^2 + \frac{1}{4}b'\left(q_1^4+q_2^4+q_3^4\right) \\ & +\frac{1}{6}c\left(q_1^2+q_2^2+q_3^2\right)^3 \\ & +\frac{1}{6}c'\left(q_1^2+q_2^2+q_3^2\right)\left(q_1^2q_2^2+q_1^2q_3^2+q_2^2q_3^2\right) \\ & +\frac{1}{6}c''\left(q_1^6+q_2^6+q_3^6\right) + \lambda_1 e_a\left(q_1^2+q_2^2+q_3^2\right) \\ & +\lambda_2\left[\sqrt{3}e_o\left(q_1^2-q_2^2\right) - e_t\left(q_1^2+q_2^2-2q_3^2\right)\right] \\ & +\lambda_3\left(e_4q_2q_3+e_5q_1q_3+e_6q_1q_2\right) \\ & +\frac{1}{4}\left(C_{11}^o-C_{12}^o\right)\left(e_o^2+e_t^2\right) + \frac{1}{6}\left(C_{11}^o+2C_{12}^o\right)e_a^2 \\ & +\frac{1}{2}C_{44}^o\left(e_4^2+e_5^2+e_6^2\right). \end{aligned} \tag{A1}$$

$q_1 - q_3$ are order parameter components, a, b, c, etc., are normal Landau coefficients, Θ_s is the saturation temperature for the order parameter, T_c is the critical temperature, λ_1,λ_2,λ_3 are coupling coefficients, C_{11}^o, C_{12}^o, C_{44}^o are bare elastic constants, and e_4, e_5, e_6 are strain components. The symmetry-adapted strains e_a, e_o, and e_t are combinations of the linear strain components e_1, e_2, and e_3, as

$$e_a = (e_1+e_2+e_3), \tag{A2}$$

$$e_o = (e_1-e_2), \tag{A3}$$

$$e_t = \frac{1}{\sqrt{3}}(2e_3-e_1-e_2). \tag{A4}$$

Space groups, nonzero order parameter components, and lattice vectors for the symmetry subgroups of $Fm\bar{3}m$ associated with Γ_4^- are listed in full in Table II. Order parameter components for the $R3m$ structure are $q_1 = q_2 = q_3 \neq 0$, and Eq. (A1) reduces to

$$\begin{aligned} G = {} & \frac{3}{2}a\Theta_s\left[\coth\left(\frac{\Theta_s}{T}\right) - \coth\left(\frac{\Theta_s}{T_c}\right)\right]q_1^2 + \frac{9}{4}bq_1^4 + \frac{3}{4}b'q_1^4 \\ & +\frac{9}{2}cq_1^6 + \frac{3}{2}c'q_1^6 + \frac{1}{2}c''q_1^6 \\ & +3\lambda_1 e_a q_1^2 + \lambda_3 q_1^2(e_4+e_5+e_6) \\ & +\frac{1}{4}\left(C_{11}^o-C_{12}^o\right)\left(e_o^2+e_t^2\right) + \frac{1}{6}\left(C_{11}^o+2C_{12}^o\right)e_a^2 \\ & +\frac{1}{2}C_{44}^o\left(e_4^2+e_5^2+e_6^2\right). \end{aligned} \tag{A5}$$

If reference axes X, Y, and Z are chosen as being parallel to the cubic crystallographic axes, the nonzero strain components are given by

$$e_1 = e_2 = e_3 = \frac{a-a_o}{a_o}, \tag{A6}$$

$$e_4 = e_5 = e_6 = \frac{a}{a_o}\cos\alpha \approx \cos\alpha, \tag{A7}$$

where a_o is the reference parameter of the cubic structure extrapolated into the rhombohedral stability field, a is the lattice parameter of the rhombohedral structure, and α is its (pseudocubic) lattice angle. The equilibrium condition $\partial G/\partial e = 0$ gives relationships between strains and order parameter components as

$$e_a = -\frac{3\lambda_1 q_1^2}{\frac{1}{3}\left(C_{11}^o+2C_{12}^o\right)}, \tag{A8}$$

$$e_o = e_t = 0, \tag{A9}$$

$$e_4 = e_5 = e_6 = -\frac{\lambda_3 q_1^2}{C_{44}^o}. \tag{A10}$$

These relationships are used here to determine the thermodynamic character of the cubic-rhombohedral transition. Cell parameter data from single crystal neutron diffraction [17] and x-ray powder diffraction [7] are reproduced in Fig. 5(a). Normally, a fit of the function [67–71]

$$a_o = a_1 + a_2\Theta_{so}\coth\left(\frac{\Theta_{so}}{T}\right) \tag{A11}$$

(where Θ_{so} is a saturation temperature for thermal expansion) is used to obtain the reference cubic lattice parameter, but

TABLE II. Space groups, nonzero order parameter components, and lattice vectors [origin = (0,0,0)], for the symmetry subgroups of $Fm\bar{3}m$ associated with active representation Γ_4^-, as obtained from the group theory program ISOTROPY [66].

Space group	Order parameter components	Relationships between order parameter components	Lattice vectors
$Fm\bar{3}m$	000		(0,0,0)(0,0,0)(0,0,0)
$I4mm$	$q_1$00		(0,1/2,1/2)(0,−1/2,1/2)(1,0,0)
$Imm2$	$q_1q_2$0	$q_1 = q_2$	(−1/2,1/2,0)(0,0,1)(1/2,1/2,0)
$R3m$	$q_1q_2q_3$	$q_1 = q_2 = q_3$	(−1/2,1/2,0)(0,−1/2,1/2)(1,1,1)
Cm	$q_1q_2$0	$q_1 \neq q_2$	(−1,0,0)(0,0,1)(1/2,1/2,0)
Cm	$q_1q_2q_3$	$q_1 = q_2 \neq q_3$	(1/2,1/2,1)(−1/2,1/2,0)(−1/2,−1/2,0)
$P1$	$q_1q_2q_3$	$q_1 \neq q_2 \neq q_3$	(0,1/2,1/2)(1/2,0,1/2)(1/2,1/2,0)

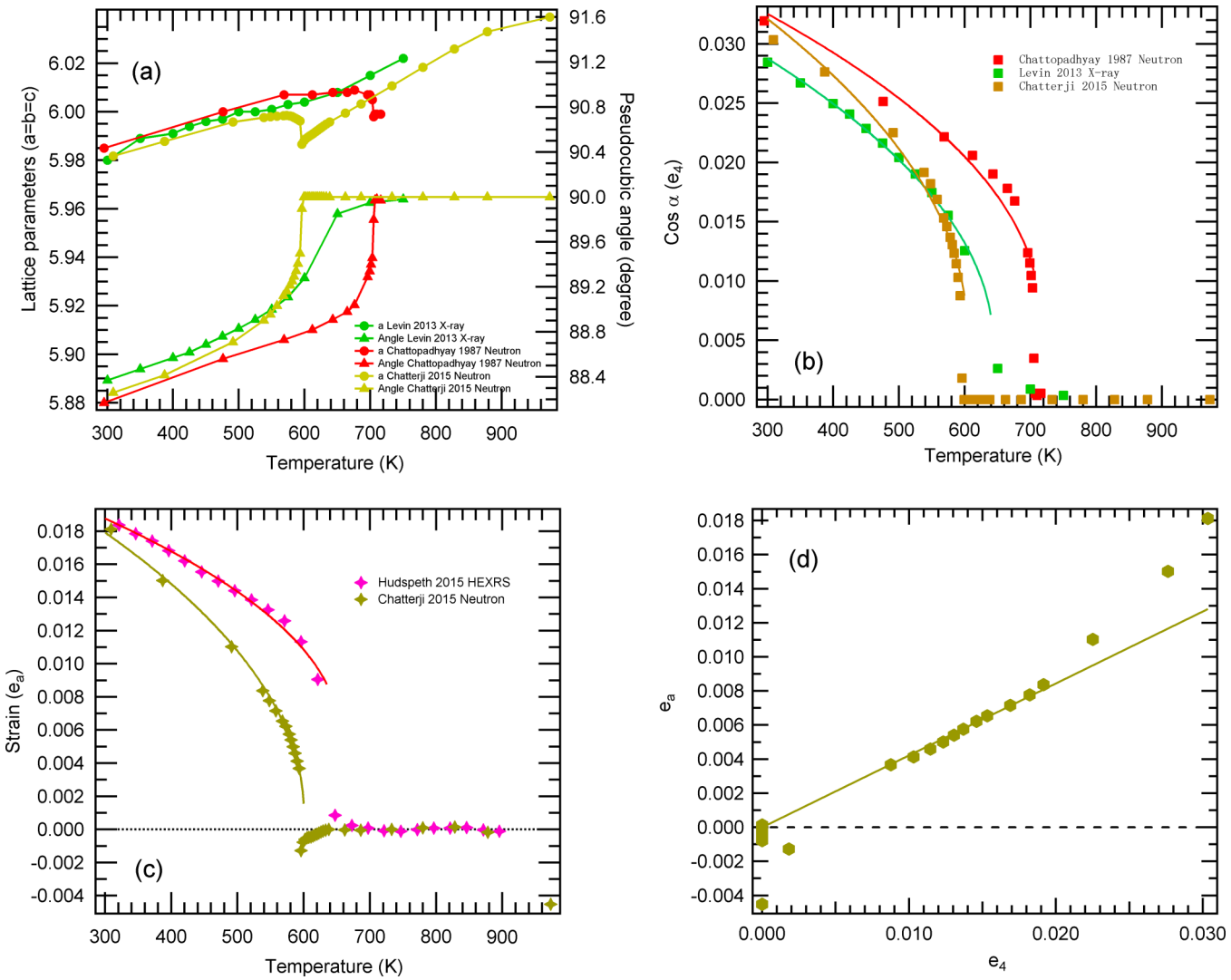

FIG. 5. Strain analysis of the $Fm\bar{3}m$-$R3m$ transition in GeTe, showing weakly first order character. (a) Cell parameter variations compiled from the literature. Straight lines fit to data points for a at the highest temperatures represent the variations of a_o extrapolated to lower temperatures. (b) Curves through the data for $\cos\alpha(\sim e_4 \propto q_1^2)$ are fits of Eq. (A12), with T_{tr} fixed at values specified in the original work and values of the fit parameters given in Table III. (c) Curves through the data for $e_a(\propto q_1^2)$ are fits of Eq. (A12), with parameters given in Table III. (d) e_a does not scale linearly with e_4 as expected from Eqs. (A8) and (A10) over the entire range.

there are insufficient data in the stability field of the cubic phase for this. However, variations of the shear strain e_4 are to good approximation given by $\cos\alpha$ and are consistent with the known, weakly first order character of the transition [Fig. 5(b)]. Added to Figs. 5(a) and 5(b) are data from the study of Chatterji *et al.* [16] which were not shown in the original paper, and from Hudspeth *et al.* [15] obtained using synchrotron x-ray powder diffraction. The latter have been used to yield fits of Eq. (A11) for a_o and, hence, to determine the values of e_a which are given in Fig. 5(c). From Eqs. (A8) and (A10), e_a and e_4 are expected to be linearly dependent but this appears not to be the case within reasonable experimental uncertainty [Fig. 5(d)]. Either there is additional higher order coupling with one or other of the strains, i.e., such as $\lambda e\, Q^4$, or one order parameter alone is not sufficient to describe the overall transformation behavior.

As in the case of the α-β transition in quartz [72] the evolution of the order parameter is expected to follow the standard Landau solution for a first-order transition:

$$Q^2 = \frac{2}{3}Q_o^2\left\{1 + \left[1 - \frac{3}{4}\left(\frac{T - T_c}{T_{tr} - T_c}\right)\right]^{1/2}\right\}, \qquad \text{(A12)}$$

where Q_o is the discontinuity in the order parameter at the transition temperature T_{tr}. The difference between T_{tr} and the critical temperature T_c is a measure of how far the transition is from being thermodynamically continuous and, although this should include the saturation temperature from Eq. (A5), it is usually adequate to ignore it in fitting data above room temperature. Figures 5(b) and 5(c) show fits of a function of the form of Eq. (A12) to data for e_4 and e_a derived from the lattice parameters of Levin *et al.* [7], Chatterji *et al.* [16], and Hudspeth *et al.* [15]. T_{tr} was fixed at the experimental values and the resulting fit parameters are listed in Table III. Just as found for the first order transition at compositions towards the Sn-rich end of the $Sn_xGe_{1-x}Te$ solid solution [18], the Landau

TABLE III. Fit parameters from Figure 5 using Equation (A12).

Source of data	$\cos\alpha_o/e_{ao}$	T_{tr}(K) (fixed)	T_c(K)	$T_{tr} - T_c$(K)
Chattopadhyay and Boucherle [17]	$\cos\alpha_o = 0.0109$	705	680	25
Chatterji *et al.* [16]	$\cos\alpha_o = 0.0086$	600	589	11
Levin *et al.* [7] x ray	$\cos\alpha_o = 0.0070$	640	630	10
Chatterji *et al.* [16]	$e_{ao} = 0.0015$	600	599	1
Hudspeth *et al.* [15]	$e_{ao} = 0.0088$	635	581	54

solution provides a good representation of the strain variations. Although the transition temperature varies between samples, the pattern of strain evolution is similar and values of $(T_{tr} - T_c)$ fall in the range 1–50 K. Changes of T_{tr} between samples of GeTe are widely attributed to the effects of changing stoichiometry (e.g., Ref. [17]), and might also contribute to changes in the strength of strain/order parameter coupling or changes in the thermodynamic character of the transition, but there are insufficient data to test this possibility systematically through correlations of $(T_{tr} - T_c)$ with the value of T_{tr}, say.

[1] M. Wuttig and N. Yamada, Nat. Mater. **6**. 824 (2007).
[2] G. Bruns, P. Merkelbach, C. Schlockermann, M. Salinga, M. Wuttig, T. D. Happ, J. B. Philipp, and M. Kund, Appl. Phys. Lett. **95**, 043108 (2009).
[3] A.V. Kolobov, M. Krbal, P. Fons, J. Tominaga, and T. Uruga, Nat. Chem. **3**, 311 (2011).
[4] X. Zhou, W. Dong, H. Zhang, and R. E. Simpson, Sci. Rep. **5**, 11150 (2015).
[5] P. Nukala, R. Agarwal, X. Qian, M. H. Jang, S. Dhara, K. Kumar, A. T. C. Johnson, J. Li, and R. Agarwal, Nano Lett. **14**, 2201 (2014).
[6] G. J. Snyder and E. S. Toberer, Nat. Mater. **7**, 105 (2008).
[7] E. M. Levin, M. F. Besser, and R. Hanus, J. Appl. Phys. **114**, 083713 (2013).
[8] M. J. Polking, J. J. Urban, D. J. Milliron, H. Zheng, E. Chan, M. A. Caldwell, S. Raoux, C. F. Kisielowski, J. W. Ager, III, R. Ramesh, and A. P. Alivisatos, Nano Lett. **11**, 1147 (2011).
[9] M. Chen, K. A. Rubin, and R. W. Barton, Appl. Phys. Lett. **49**, 502 (1986).
[10] A. H. Edwards, A. C. Pineda, P. A. Schultz, M. G. Martin, A. P. Thompson, H. P. Hjalmarson, and C. J. Umrigar, Phys. Rev. B **73**, 045210 (2006).
[11] J.-P. Gaspard, A. Pellegatti, F. Marinelli, and C. Bichara, Philos. Mag. B **77**, 727 (1998).
[12] J. Y. Raty, V. Godlevsky, Ph. Ghosez, C. Bichara, J. P. Gaspard, and J. R. Chelikowsky, Phys. Rev. Lett. **85**, 1950 (2000).
[13] P. Fons, A. V. Kolobov, M. Krbal, J. Tominaga, K. S. Andrikopoulos, S. N. Yannopoulos, G. A. Voyiatzis, and T. Uruga, Phys. Rev. B **82**, 155209 (2010).
[14] T. Matsunaga, P. Fons, A. V. Kolobov, J. Tominaga, and N. Yamada, Appl. Phys. Lett. **99**, 231907 (2011).
[15] J. M. Hudspeth, T. Chatterji, S. J. Billinge, and S. A. Kimber, arXiv:1506.08944.
[16] T. Chatterji, C. M. N. Kumar, and U. D. Wdowik, Phys. Rev. B **91**, 054110 (2015).
[17] T. Chattopadhyay and J. Boucherle, J. Phys. C: Solid State Phys. **20**, 1431 (1987).
[18] E. Steigmeier and G. Harbeke, Solid State Commun. **8**, 1275 (1970).
[19] K. M. Rabe and J. D. Joannopoulos, Phys. Rev. B **36**, 6631 (1987).
[20] R. Clarke, Phys. Rev. B **18**, 4920 (1978).
[21] S. Sugai, K. Murase, T. Tsuchihira, and H. Kawamura, J. Phys. Soc. Jpn. **47**, 539 (1979).
[22] U. D. Wdowik, K. Parlinski, S. Rols, and T. Chatterji, Phys. Rev. B **89**, 224306 (2014).
[23] A. V. Kolobov, D. J. Kim, A. Giussani, P. Fons, J. Tominaga, R. Calarco, and A. Gruverman, APL Mater. **2**, 066101 (2014).
[24] A. S. Nowick and B. S. Berry, *Anelastic Relaxation in Crystalline Solids* (Academic, New York, 1972).
[25] M. A. Carpenter and C. J. Howard, Acta Crystallogr. Sect. B **65**, 147 (2009).
[26] R. E. A. McKnight, C. J. Howard, and M. A. Carpenter, J. Phys.: Condens. Matter **21**, 015901 (2009).
[27] A. S. Migliori and J. L. Sarrao, *Resonant Ultrasound Spectroscopy: Applications to Physics, Materials Measurements and Nondestructive Evaluation* (Wiley, New York,1997).
[28] R. E. A. McKnight, M. A. Carpenter, T. W. Darling, A. Buckley, and P. A. Taylor, Am. Mineral. **92**, 1665 (2007).
[29] R. E. A. McKnight, T. Moxon, A. Buckley, P. A. Taylor, T. W. Darling, and M. A. Carpenter, J. Phys.: Condens. Matter **20**, 075229 (2008).
[30] A. Migliori and J. D. Maynard, Rev. Sci. Instrum. **76**, 121301 (2005).
[31] M. A. Carpenter and E. K. H. Salje, Eur. J. Mineral. **10**, 693 (1998).
[32] I. Hatta and K. L. I. Kobayashi, Solid State Commun. **22**, 775 (1977).
[33] M. A. Carpenter, *Physical Properties and Thermodynamic Behaviour of Minerals*, NATO ASI Ser. C, Vol. 225, edited by E. K. H. Salje (Reidel, Dordrecht, 1988), pp. 265–323.
[34] I. Hatta and W. Rehwald, J. Phys. C: Solid State Phys. **10**, 2075 (1977).
[35] W. Rehwald and G. K. Lang, J. Phys. C: Solid State Phys. **8**, 3287 (1975).
[36] T. Seddon, J. M. Farley, and G. A. Saunders, Solid State Commun. **17**, 55 (1975).
[37] T. Seddon, S. C. Gupta, and G. A. Saunders, Phys. Lett. A **56**, 45 (1976).
[38] N. Kh. Abrikosov, M. A. Korzhuev, L. A. Petrov, O. A. Teplov, and G. K. Demenckii, Inorg. Mater. **19**, 334 (1983) [Inorg. Mater. **19**, 370 (1983)].
[39] J. C. Slonczewski and H. Thomas, Phys. . B **1**, 3599 (1970).
[40] R. I. Thomson, T. Chatterji, and M. A. Carpenter, J. Phys.: Condens. Matter **26**, 146001 (2014).

[41] L. J. Spalek, S. S. Saxena, C. Panagopoulos, T. Katsufuji, J. A. Schiemer, and M. A. Carpenter, Phys. Rev. B **90**, 054119 (2014).
[42] J. Schiemer, L. J. Spalek, S. S. Saxena, C. Panagopoulos, T. Katsufuji, and M. A. Carpenter, Europhys. Lett. **109**, 57004 (2014).
[43] N. J. Perks, Z. Zhang, R. J. Harrison, and M. A. Carpenter, J. Phys.: Condens. Matter **26**, 505402 (2014).
[44] M. A. Carpenter, E. K. H. Salje, and C. J. Howard, Phys. Rev. B **85**, 224430 (2012).
[45] G. F. Nataf, Q. Li, Y. Liu, R. L. Withers, S. L. Driver, and M. A. Carpenter, J. Appl. Phys. **113**, 124102 (2013).
[46] R. J. Harrison, S. A. Redfern, and J. Street, Am. Mineral. **88**, 574 (2003).
[47] R. J. Harrison and S. A. T. Redfern, Phys. Earth Planet Int. **134**, 253 (2002).
[48] R. J. Harrison, S. A. T. Redfern, and E. K. H. Salje, Phys. Rev. B **69**, 144101 (2004).
[49] M. Daraktchiev, R. J. Harrison, E. H. Mountstevens, and S. A. T. Redfern, Mater. Sci. Eng. A **442**, 199 (2006).
[50] M. A. Carpenter and Z. Zhang, Geophys. J. Int. **186**, 279 (2011).
[51] E. K. H. Salje, X. Ding, Z. Zhao, T. Lookman, and A. Saxena, Phys. Rev. B **83**, 104109 (2011).
[52] M. A. Carpenter, J. Phys.: Condens. Matter **27**, 263201 (2015).
[53] V. L. Deringer, M. Lumeii, R. P. Stoffel, and R. Dronskowski, Chem. Mater. **25**, 2220 (2013).
[54] J. A. Schiemer, R. L. Withers, Y. Liu, and M. A. Carpenter, Chem. Mater. **25**, 4436 (2013).
[55] M. A. Carpenter, C. J. Howard, R. E. A. McKnight, A. Migliori, J. B. Betts, and V. Fanelli, Phys. Rev. B **82**, 134123 (2010).
[56] J. D. Axe and G. Shirane, Phys. Rev. B **1**, 342 (1970).
[57] E. Pytte, Phys. Rev. B **1**, 924 (1970).
[58] E. Pytte, in *Structural Phase Transitions and Soft Modes*, edited by E. J. Samuelsen, J. Anderson, and J. Feder (NATO ASI Norway. Scandinavian University Books, Oslo, 1971), p. 151.
[59] U. T. Höchli, Phys. Rev. B **6**, 1814 (1972).
[60] M. A. Carpenter, J. F. J. Bryson, G. Catalan, S. J. Zhang, and N. J. Donnelly, J. Phys.: Condens. Matter **24**, 045902 (2012).
[61] O. Aktas, E. K. H. Salje, S. Crossley, G. I. Lampronti, R. W. Whatmore, N. D. Mathur, and M. A. Carpenter, Phys. Rev. B **88**, 174112 (2013).
[62] R. Mackeviciute, V. Goian, S. Greicius, R. Grigalaitis, D. Nuzhnyy, J. Holc, J. Banys, and S. Kamba, J. Appl. Phys. **117**, 084101 (2015).
[63] F. Kadlec, C. Kadlec, P. Kužel, and J. Petzelt, Phys. Rev. B **84**, 205209 (2011).
[64] E. K. H. Salje, Chem. Phys. Chem **11**, 940 (2010).
[65] D. D. Viehland and E. K. H. Salje, Adv. Phys. **63**, 267 (2014).
[66] H. T. Stokes, D. M. Hatch, and B. J. Campbell, ISOTROPY, http://stokes.byu.edu/isotropy.html (2005).
[67] M. A. Carpenter, J. Bryson, G. Catalan, and C. Howard, J. Phys.: Condens. Matter **24**, 045901 (2012).
[68] E. Salje, B. Wruck, and H. Thomas, Z. Phys. B **82**, 399 (1991).
[69] H.-W. Meyer, M. A. Carpenter, A. Graeme-Barber, P. Sondergeld, and W. Schranz, Eur. J. Mineral. **12**, 1139 (2000).
[70] H.-W. Meyer, S. Marion, P. Sondergeld, M. A. Carpenter, K. S. Knight, S. A. T. Redfern, and M. T. Dove, Am Minera.l **86**, 566 (2001).
[71] P. Sondergeld, W. Schranz, A. V. Kityk, M. A. Carpenter, and E. Libowitzky, Phase Trans. **71**, 189 (2000).
[72] M. A. Carpenter, E. K. H. Salje, A. Graeme-Barber, B. Wruck, M. T. Dove, and K. S. Knight, Am. Mineral. **83**, 2 (1998).